Chem Soc Rev

This article was published as part of the

2008 Chemistry at Surfaces issue

Reviewing the latest developments in surface science

All authors contributed to this issue in honour of the 2007 Nobel Prize winner Professor Gerhard Ertl

Please take a look at the issue 10 table of contents to access the other reviews

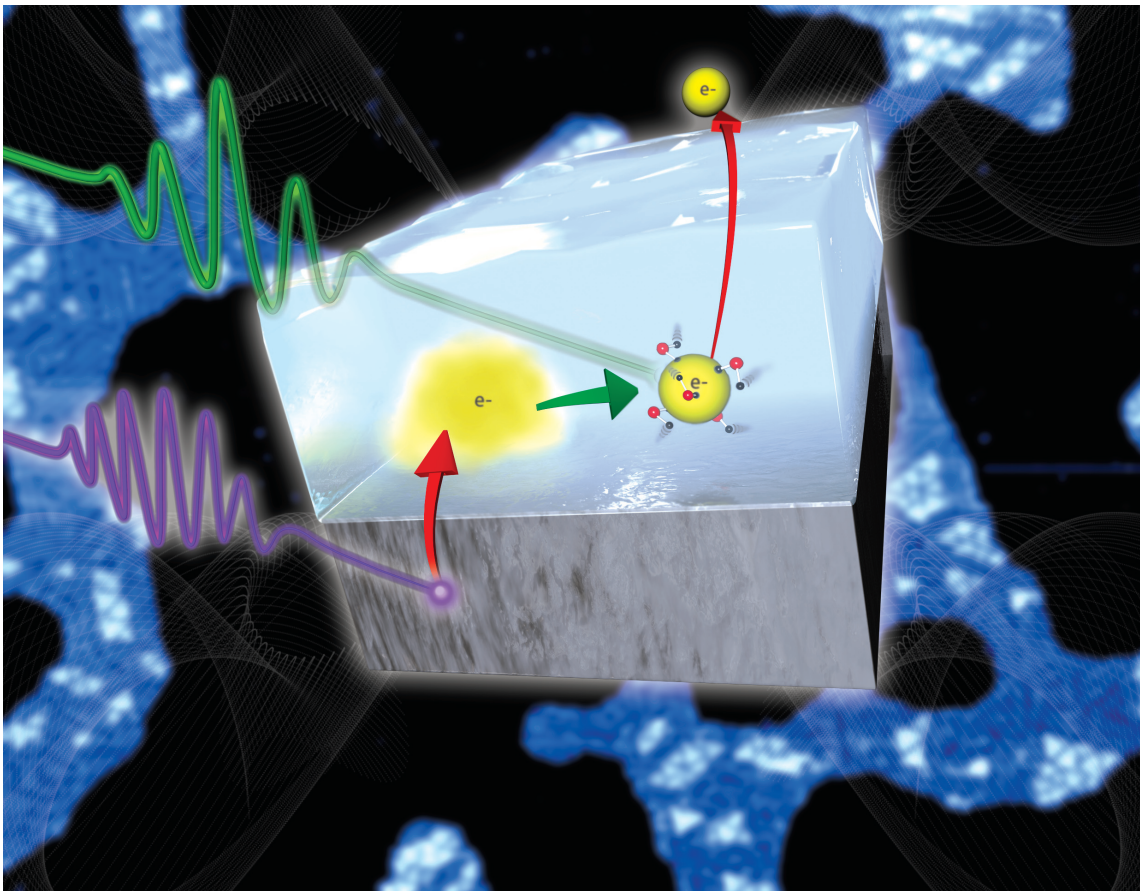

Chem Soc Rev

Chemical Society Reviews

www.rsc.org/chemsocrev

Volume 37 | Number 10 | October 2008 | Pages 2141–2360

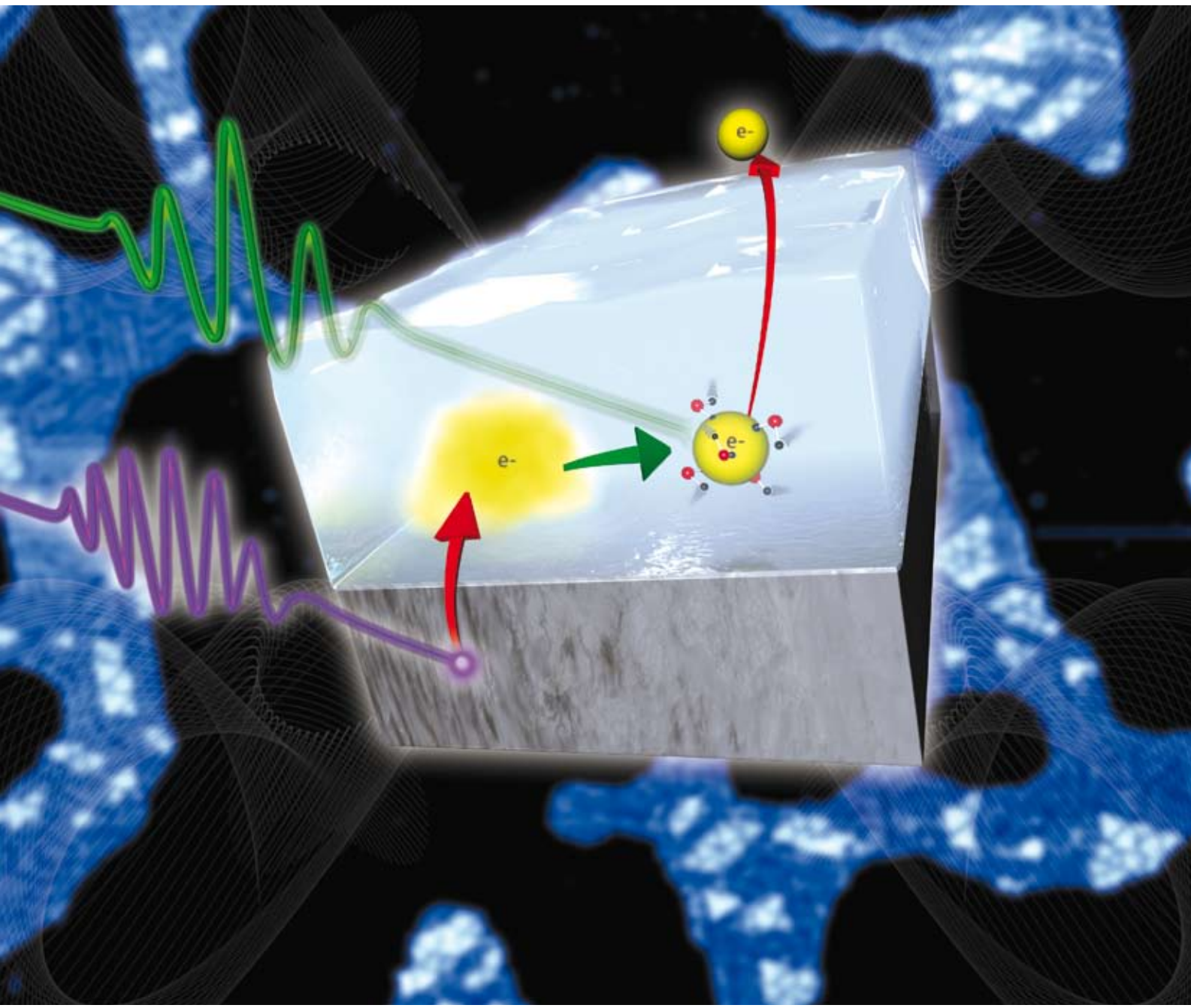

ISSN 0306-0012

RSC Publishing

THEMATIC ISSUE: CHEMISTRY AT SURFACES
Guest editors: Hans-Peter Steinrück, Jörg Libuda and Sir David A. King

0306-0012(2008)37:10;1-U

A surface science approach to ultrafast electron transfer and solvation dynamics at interfaces†

Julia Stähler, Uwe Bovensiepen, Michael Meyer and Martin Wolf

Received 5th June 2008
First published as an Advance Article on the web 15th August 2008
DOI: 10.1039/b800257f

Excess electrons in polar media, such as water or ice, are screened by reorientation of the surrounding molecular dipoles. This process of electron solvation is of vital importance for various fields of physical chemistry and biology as, for instance, in electrochemistry or photosynthesis. Generation of such excess electrons in bulk water involves either photoionization of solvent molecules or doping with *e.g.* alkali atoms, involving possibly perturbing interactions of the system with the parent-cation. Such effects are avoided when using a surface science approach to electron solvation: in the case of polar adsorbate layers on metal surfaces, the substrate acts as an electron source from where photoexcited carriers are injected into the adlayer. Besides the investigation of electron solvation at such interfaces, this approach allows for the investigation of heterogeneous electron transfer, as the excited solvated electron population continuously decays back to the metal substrate. In this manner, electron transfer and solvation processes are intimately connected at any polar adsorbate–metal interface. In this *tutorial review*, we discuss recent experiments on the ultrafast dynamics of photoinduced electron transfer and solvation processes at amorphous ice–metal interfaces. Femtosecond time-resolved two-photon photoelectron spectroscopy is employed as a direct probe of the electron dynamics, which enables the analysis of all elementary processes: the charge injection across the interface, the subsequent electron localization and solvation, and the dynamics of electron transfer back to the substrate. Using surface science techniques to grow and characterize various well-defined ice structures, we gain detailed insight into the correlation between adsorbate structure and electron solvation dynamics, the location (bulk *versus* surface) of the solvation site, and the role of the electronic structure of the underlying metal substrate on the electron transfer rate.

1. Introduction

When an excess charge is brought into a polarizable medium, it is screened by the (frequency-dependent) dielectric response of the environment. This screening process of electrons or ions is referred to as solvation, which plays a key role in various areas of physical chemistry and biology.[1] Such excess electrons in ammonia or water are known to form electron–solvent complexes[2,3] and are referred to as ammoniated[4] or hydrated[5] electrons. The dynamics of the formation and subsequent energetic stabilization of these solvated electron complexes by molecular rearrangement occurs on a femtosecond time scale and has been studied in bulk water by ultrafast laser spectroscopy.[6,7] However, as the excess electrons are generated

Freie Universität Berlin, Fachbereich Physik, Arnimallee 14, 14195 Berlin, Germany. E-mail: wolf@physik.fu-berlin.de
† Part of a thematic issue covering reactions at surfaces in honour of the 2007 Nobel Prize winner Professor Gerhard Ertl.

Uwe Bovensiepen, Michael Meyer, Julia Stähler and Martin Wolf

Research team at the Freie Universität Berlin studying ultrafast interfacial electron transfer and solvation dynamics (from left to right): Uwe Bovensiepen, Michael Meyer, Julia Stähler and Martin Wolf.
Julia Stähler is currently a postdoc at the University of Oxford and received a PhD from the FU Berlin for studies of electron solvation dynamics at polar adsorbate–metal interfaces. This work is now developed in new directions by Michael Meyer, who is working on his PhD thesis. The research team is lead by the senior scientists Uwe Bovensiepen and Martin Wolf. The laboratory at the Freie Universität Berlin studies a broad range of ultrafast phenomena in solids and at surfaces ranging from highly correlated electrons to surface chemical reactions.

with the aid of photoionization of solvent molecules or doping with *e.g.* alkali atoms or salts, the achievement of microscopic insight into the primary steps of electron solvation is often hampered by the interaction of the nascent photoexcited electron with the corresponding cation, which becomes also solvated on similar timescales. Also, the binding energy of the hydrated electron cannot be determined directly in bulk water and is obtained as 3.2 eV from extrapolation of the vertical binding energies of $(H_2O)_n^-$ clusters to infinite cluster size.[8] Such water anion-clusters of defined size n are therefore frequently used as model systems to study electron solvation dynamics in finite systems.[9] Nevertheless, it is currently controversially discussed whether the excess electron resides in the bulk or at the surface of these clusters[9,10] and in how far the transition between a surface to an interior site depends on the cluster size and its structure and temperature. The actual molecular structure of the clusters is a key ingredient to settle this question,[10] but is usually unknown in molecular beam experiments.

In this article we present an alternative concept to address fundamental questions of electron solvation dynamics, which is based on a surface science approach.[11–13] Using well-characterized amorphous ice structures adsorbed on single crystal metal surfaces, the dynamics of photoinjected electrons in the ice is monitored by femtosecond (fs) time- and angle-resolved two-photon photoelectron spectroscopy (2PPE).[14] This allows direct probing of the transient changes of the electron's binding energy and its degree of localization during the initial steps of the solvation process without interference with the photohole, which is completely screened by the metal electrons.[15] As will be discussed in detail further below, the combination of surface science techniques like low-temperature scanning tunneling microscopy (LT-STM) with ultrafast 2PPE spectroscopy enables the analysis of the correlation between differently prepared ice structures and the corresponding electron solvation dynamics.[16] Also, the location of the solvation site in the interior of the ice or at the ice–vacuum interface can be probed by Xe overlayer experiments. Note, that solvation dynamics at metal interfaces have also been studied for other polar adlayers like alcohols,[17] nitrils,[11,18] and ammonia.[19,20]

Moreover, investigation of electron solvation dynamics at molecule–metal interfaces bridges to the important area of interfacial electron transfer (ET), which is of vital importance in technologically highly relevant fields.[1,21] Examples are dye-sensitized solar (Grätzel) cells,[22] organic optoelectronic and nanoscale molecular devices,[23,24] where charge injection and electronic coupling between a conducting electrode and a molecular system is of key relevance.[1] Detailed measurements of the electron transfer rate at different ice–metal interfaces (D_2O/Cu(111) and Ru(001), respectively) reveal the role of the substrate electronic structure in adsorbate–substrate, charge transfer, which competes with the localization and solvation dynamics in the ice. Thus electron transfer and solvation processes at polar adsorbate–metal interfaces provide a well defined model system to elucidate fundamental questions regarding charge transport in molecular electronic devices.

While 2PPE spectroscopy is an ideal tool to directly access the charge transfer and solvation dynamics of the excess electron itself, the corresponding nuclear rearrangements of the solvation shell are only indirectly monitored *via* the transient changes of the electron binding energy. Direct structural information could be obtained, for example, by infrared spectroscopy, as has been nicely demonstrated for small water anion clusters.[25] However, application of vibrational spectroscopy to solvation dynamics at interfaces remains a challenge due to the small concentration of electron–water complexes at the interface, which are photoexcited at low densities to exclude interactions between these electrons. In this article we will thus focus on studies using the nearly background free 2PPE technique.

In the following, we will first briefly review the basic mechanisms and elementary processes of the electron dynamics at amorphous ice–metal interfaces using D_2O/Cu(111) as an example (section 2). In section 3 we provide a detailed overview on the role of the morphology and structure of the ice (*e.g.* adsorbed D_2O clusters *versus* closed ice layers) on the resulting solvation and relaxation dynamics as well as on the electron solvation site. Finally, we compare the dynamics in ice layers on Cu(111) and Ru(001), which exhibit different surface electronic band structures. We find different regimes of electron transfer, which result from the competition between the electron solvation process and the charge transfer back to the metal substrate. The surface science approach to interfacial electron transfer and solvation dynamics provides thus detailed insights into elementary processes which are complementary to related studies in the gas or liquid phases.

2. Elementary process of electron transfer and solvation

The ultrafast electron dynamics at ice–metal interfaces are characterized by charge injection into the adsorbate layer, localization at favorable sites, followed by energetic stabilization, and electron transfer back to the metal substrate. These elementary processes will be introduced in the following. We start with the presentation of the time- and angle-resolved 2PPE data of amorphous multilayers of D_2O adsorbed on a Cu(111) single crystal surface at 100 K. Based on these experimental evidences, the fundamental steps of electron dynamics at ice–metal interfaces will be identified and discussed.

The principle of time-resolved 2PPE spectroscopy is schematically illustrated in Fig. 1b. Metal electrons are excited from below the Fermi level E_F into unoccupied, bound states below the vacuum level E_{vac} by a first, femtosecond laser pulse $h\nu_1$ (pump). The subsequent dynamics of the excited electron population (step 1–4, see Fig. 1b) are then monitored by a second, time-delayed laser pulse $h\nu_2$ (probe) that excites the electrons above E_{vac} where their kinetic energy is analyzed in an electron time-of-flight (TOF) spectrometer.

A representative 2PPE measurement of an amorphous multilayer D_2O on Cu(111) is shown in Fig. 1a. The photoemission intensity is depicted in a false color representation and plotted as a function of intermediate state energy $E - E_F = E_{kin} + \Phi - h\nu_2$ with respect to the Fermi level of the metal and as a function of pump–probe time delay. The spectrum exhibits two features, a broad continuum e_{CB} and a distinct

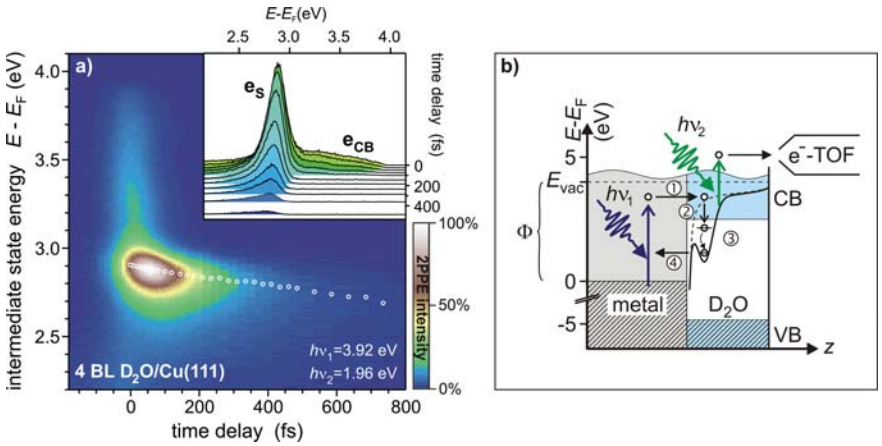

Fig. 1 (a) Time-resolved 2PPE of an amorphous multilayer of D_2O/Cu(111). Two features are discerned: a broad, short-lived continuum e_{CB} resulting from conduction band electrons in the ice layer and a distinct peak e_S that is shifting towards the Fermi level with increasing time delay and which originates from solvated electrons in the adlayer. (Modified from ref. 15 with permission. Copyright 2003, the American Chemical Society.) (b) 2PPE scheme and elementary processes. Metal electrons are excited by a first laser pulse $h\nu_1$ and injected into the D_2O layer *via* the ice conduction band (step 1). They localize in the adlayer (step 2) and are energetically stabilized by molecular rearrangement (step 3). Concurrently, the electron population decays back to the substrate (step 4). These electron dynamics are monitored by a second, time-delayed laser pulse $h\nu_2$, which excites the electrons to the vacuum where their kinetic energy is analyzed by an electron time-of-flight spectrometer. (Reproduced from ref. 12 with permission. Copyright 2005, Elsevier B.V.)

peak e_S that is shifting down to lower energies with increasing time delay (open circles). As apparent from the inset, the intensity of these two spectral signatures decreases with increasing time delay (right axis). However, e_{CB} decays considerably faster than the long-living feature e_S.

Insight into the character of the two spectral signatures e_{CB} and e_S is achieved by time- *and* angle-resolved 2PPE spectroscopy (Fig. 2). By variation of the emission angle of the photoelectrons from the sample (right panel), it is possible to measure their parallel momentum, which yields information on the degree of lateral localization of the electronic state. The parallel momentum

$$k_{\parallel}(\varphi, E_{\mathrm{kin}}) = \sin\varphi \cdot \sqrt{\frac{2m_e}{\hbar} \cdot E_{\mathrm{kin}}} \qquad (1)$$

depends on the angle φ between the surface normal and the emission angle as illustrated by the right panel of Fig. 2. The analysis of the time- and angle-resolved data of a multilayer D_2O/Cu(111) is shown in the left panel. The short-lived continuum e_{CB} (solid markers) exhibits a positive dispersion yielding an effective mass equal to the free electron $m_{\mathrm{eff}} = 1.0(2)\cdot m_e$, as discussed in detail in ref. 15. This dispersion indicates the delocalized character of this band. The peak e_S (open symbols), however, shifts towards lower energies with time delay and exhibits an apparently negative dispersion which becomes stronger with increasing time delay, suggesting that the electron wave function of this state becomes progressively localized, as discussed below.

Having presented typically time- and angle-resolved 2PPE experiments on amorphous D_2O layers on Cu(111), we now discuss the underlying elementary processes of charge injection, localization, energetic stabilization, and electron back transfer with the aid of Fig. 1b. As direct photoexcitation of electrons *within* the ice layer is highly improbable due to the band gap of ice of 8.2 eV,[26] all photoexcited electrons have to originate from the Cu(111) substrate (see step 1 in Fig. 1b). Because of the delocalized (free electron like) character of e_{CB}, we assign this feature to the conduction band (CB) of the ice adlayer. The rapid decay of the e_{CB} population originates from the strong electronic coupling between the delocalized conduction band electrons and the unoccupied states of the metal, which enables—on the other hand—the charge injection of excited metal electrons into the adlayer. Besides the decay of the electron population back to the substrate, CB electrons may also localize at favorable sites in the adlayer (step 2), for instance, in potential minima caused by bond angle fluctuations.[27] This charge localization is reflected by the non-positive dispersion of the spectral signature e_S. The apparently negative

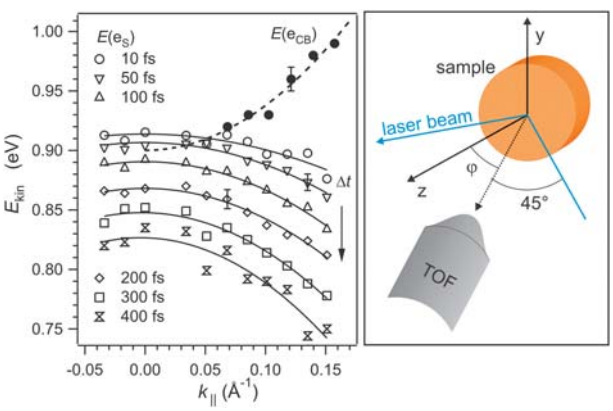

Fig. 2 Angle- and time-resolved 2PPE of D_2O/Cu(111). Left: dispersion of conduction band e_{CB} (solid markers) and solvated electrons e_S (open symbols). See text for details. (Reprinted from ref. 15 with permission. Copyright 2003, the American Chemical Society.) Right: Experimental scheme for angle-resolved measurements. Variation of the emission angle yields information about the parallel momentum of the photoelectrons and therefore about their degree of localization parallel to the surface.

dispersion of e_S is a result of the finite bandwidth, $\Delta k_{\parallel}$, of the interfacial electrons in momentum space and the experimental fact that spectra are taken at a specific angle and not a specific $k_{\parallel}$ as discussed in detail in ref. 15. The transient localization of the excess charge is driven by continuous reorientations of the surrounding polar water molecules. This wave function constriction is accompanied by an energetic stabilization of the electrons (step 3), which is reflected in the energetic shift of the e_S peak maximum as a function of pump–probe time delay.[28] As excess electron localization and energetic stabilization are characteristic properties of electron solvation in polar solvents, we assign the spectral signature e_S to solvated electrons in the amorphous ice adlayer. The population of the solvated electron state continuously decays back to the Cu(111) substrate (step 4) as indicated by the intensity decrease of e_S as a function of time delay in Fig. 1a. The charge transfer dynamics in amorphous ice layers are strongly influenced by the ice structure and the electronic properties of the metal substrate as will be shown in the following sections.

3. Correlation between ice structure and ultrafast dynamics

The ice morphology as well as the local arrangement of water molecules are important to describe the rates of energy relaxation of optically excited electrons at ice–metal interfaces. In the case of electron solvation in ice, the mobility of water molecules determines the rate of energy gain, suggesting a sensitivity of this relaxation channel to the local structure of water molecules in the hydrogen bonded network. Transfer rates of excess electrons from the ice layer to the metal substrate are determined by the electronic coupling of the interfacial electron to the substrate. Since the electron is excited to a localized state, a potential barrier forms between the localized, solvated electron and the metal substrate. The electron transfer occurs by tunneling through this barrier. Properties of the potential barrier as its height, width and shape determine the wave function overlap between donor and acceptor and hence the transfer rate. At this point the ice morphology becomes important, because the maximum distance of the excess electron may be larger for ice clusters that form on a hydrophobic substrate than for a wetting film on a hydrophilic surface of the same total coverage.

A strength of the employed surface science approach to electron transfer and solvation dynamics is the associated ability to characterize and to modify the adsorbed ice systematically. This enables the investigation of the correlation between structure and relaxation processes. These experiments have also been carried out using a single crystal Cu(111) substrate. For low D_2O coverages up to two bilayers (BL) the ice grows in clusters on Cu(111)—as on hydrophobic surfaces. This is concluded from the 2PPE spectra in the right panel of Fig. 3, which were taken for D_2O coverages of 1 BL (top) and 4 BL (bottom). The presence of the photoemission lines of the first image potential state and the occupied surface state of Cu(111) indicate regions of bare metal surface for the low coverage spectrum. However, in addition the solvated electron signature e_S is found at 2.9 eV. For mass equivalent coverages, Θ, above 2 BL these contributions of the bare metal surface vanish, and the 2PPE spectra become similar to the ones as introduced above in section 2. The time-dependent shift of the peak maximum of the solvated electron distribution (for short: peak shift) for different D_2O coverages on Cu(111) is given in the left panel. As these dynamics differ for the two ice morphologies (clusters and layers), two coverage regimes below and above 2 BL are identified. For the wetting layers ($\Theta > 2$ BL) the peak shift is independent of coverage and evolves with 0.3 eV ps^{-1}, which is slower than for ice clusters exhibiting a peak shift of 1 eV ps^{-1}. At a first glance, one might interpret the faster peak shift for clusters as a faster stabilization due to electron solvation. However, as will be shown in section 4 by a model that accounts for the competition of population decay and solvation, it is a modification of the electron transfer rate that generates this faster peak shift.

Electron transfer and solvation dynamics also depend on the binding site of the excess electron, which could either be in the bulk of an ice film or at the ice–vacuum interface, depending on the spatial distribution of attractive sites and respective population probabilities. Such an identification of the electron's binding site is a valuable input for a quantitative understanding of the data. Surface science offers a direct way to test the site by modification of the dielectric constant of the region in front of the ice surface by adsorption of, *e.g.*, Xe overlayers. Under UHV conditions and at low temperatures —Xe adsorbs on D_2O below 60 K[29]—a Xe adlayer is formed, because Xe atoms cannot be accommodated inside the water network under UHV conditions.[30] Suppose that the excess electron resides at the ice–vacuum interface before adsorption of the Xe adlayer, the 2PPE spectrum before and after Xe adsorption will vary, as the excess electron is repelled by the electron density of Xe. If the solvated electron resides in the bulk of the ice structure, the spectral signature of the electron might remain unaltered, since the solvation shell screens the excess electron from the Xe adlayer. If at all, only the net electric field of the shell could interact with the xenon.

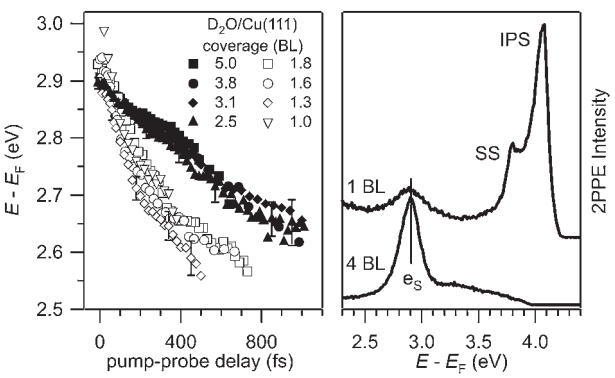

Fig. 3 Right: 2PPE spectra for 1 and 4 BL mass equivalent coverages of D_2O on Cu(111). The spectra of the 4 BL coverage exhibits two features that are attributed to the solvated electron at 2.9 eV and to the water CB up to 4.0 eV. For the 1 BL preparation two signatures of the bare Cu(111) surface are encountered: the Shockley surface state (SS) and the first image potential state (IPS). Left: time-dependent shift of the peak maximum of e_S for different coverages Θ. Two regimes are identified that are attributed to wetting layers ($\Theta > 2$ BL) and to clusters ($\Theta < 2$ BL) (Reprinted from ref. 12 with permission. Copyright 2005, Elsevier B.V.).

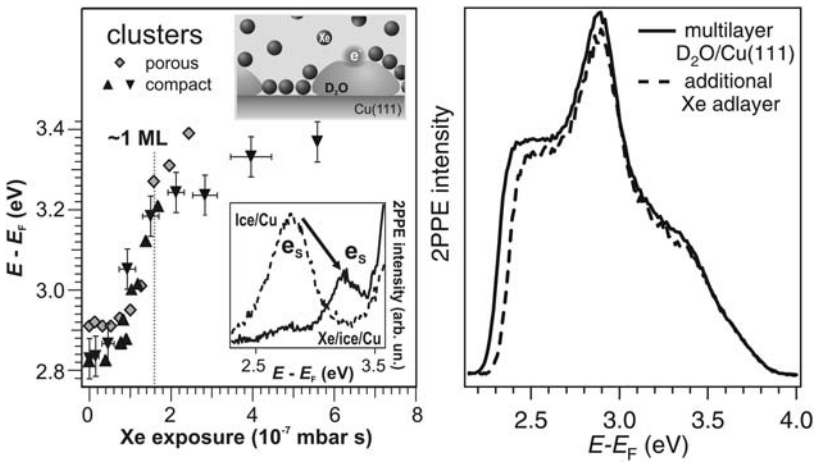

Fig. 4 Determination of the hydrated electron's binding site by Xe titration of D_2O clusters and wetting layers. Left: in case of the D_2O clusters the e_S peak changes (see bottom inset) which indicates that the electrons reside at the ice–vacuum interface. The main panel shows the peak shift as a function of Xe exposure for porous and compact amorphous D_2O clusters on Cu(111) (Reprinted from ref. 16 with permission. Copyright 2007 by the American Physical Society). Right: for the ice multilayer the peak of the hydrated electron is not modified showing that the electron resides in the film bulk; the shift of the low-energy cutoff is due to a modification of work function upon Xe adsorption (Reproduced from ref. 29 with permission from the PCCP Owner Societys).

For wetting layers of D_2O/Cu(111) the solvated electron signature in 2PPE remains unaltered upon Xe adsorption as shown in Fig. 4 (right panel). Accordingly, the electron is solvated in the bulk of wetting ice layers D_2O/Cu(111).[29] The shift of the low-energy cutoff in the spectrum results from the change of the workfunction from the one of an amorphous D_2O surface to a Xe terminated one. The situation is different for the coverage range below 2 BL where clusters are formed. As shown in the left panel of Fig. 4, the solvated electron signature e_S shifts upon adsorption of Xe by more than 0.4 eV to higher energies. In other words, the excess electron's binding energy with respect to E_{vac} is reduced, which we attribute to interaction of the solvated electron with the rare gas atoms. Thus, the electron is solvated at a surface site for ice clusters as sketched in the top inset of Fig. 4. This is contrary to the wetting ice layers where the electron resides in the bulk of the adlayer as shown above.

Beside the morphological change from clusters to wetting layers of D_2O/Cu(111), which can be explained by the D_2O–Cu interaction being comparable to hydrogen bonding, rich structural modifications of the clusters have been observed for different annealing temperatures. These have been investigated in collaboration with K. Morgenstern and coworkers using low-temperature scanning tunneling microscopy (STM).[16] This method is a unique tool to unveil local structural modifications in amorphous structures down to the molecular scale. Such a detailed structural characterization is a prerequisite to conclude on structurally induced changes of electron transfer dynamics. The top panels of Fig. 5 show low-temperature STM images of D_2O clusters on Cu(111) adsorbed at 85 K (A) and successively annealed to (a) 118 K, (b) 130 K, (c) 145 K, and flashed to 149 K. For the structures shown in panels (A) and (a) neither long range order nor defined arrangement is encountered. Thus, they represent amorphous structures. Line scans of structures depicted in panels (A) and (a) are given in panel (C) showing that the cluster heights differ on average by about one bilayer while no water desorption has been detected during heating. Analysis of all imaged clusters before and after heating results in a 40% volume reduction. We conclude that the as-grown clusters contain pores. A dosing temperature of 85 K apparently cannot lead to a dense condensation. Annealing to 118 K offers sufficient thermal energy for a collapse of the pores which explains the volume reduction.[16] In the following, we refer to these two structures as porous and compact amorphous ice clusters. For higher annealing temperatures in the narrow temperature window of 19 K, further structural transformations are observed. The transition from amorphous ice to a faceted surface (Fig. 5b), pyramidal islands (c), and finally nanocrystallites (d), depicts the continuous crystallization of the clusters. Interestingly, the well-known bilayer structure does not present a terminating surface for these crystallites, for details see ref. 31.

The defined structural modifications of D_2O/Cu(111) demonstrated here enable the investigation of the correlation between structure and electron dynamics observed by pump–probe experiments. Time-resolved 2PPE spectra were taken for all structures shown in Fig. 5 and are comprehensively discussed in ref. 19. Here, we focus on the changes upon the transition from porous to compact amorphous structures. First, all corresponding experimental results will be introduced before turning to a discussion of the correlation between structure and electron dynamics. The time-resolved data are analyzed according to the transient energy and the population of the e_S spectral signature as depicted in the top panel of Fig. 6 for compact and porous amorphous clusters. The main panel shows the transient peak position of the solvated electron distribution. We find that the peak shift spans for porous clusters an energy range of 340 meV within 300 fs, which is larger than for compact clusters (200 meV). After 300 fs, the electrons reach an equivalent state of solvation for both structures, because they exhibit the same binding energy

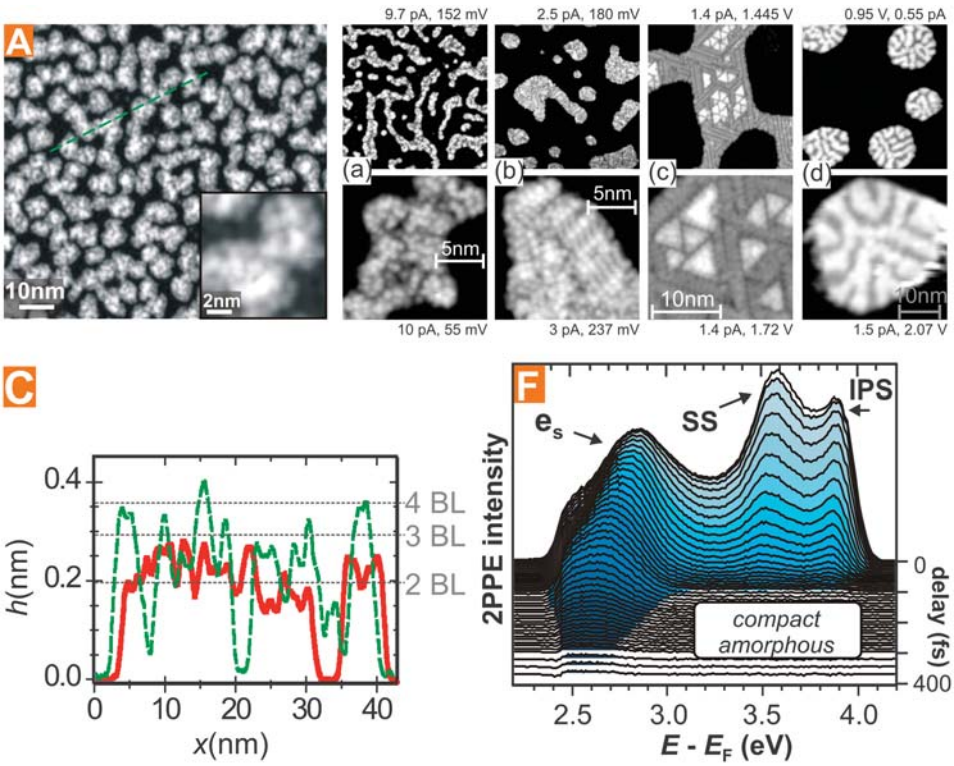

Fig. 5 Ice clusters D_2O/Cu(111) as imaged by low temperature STM at 5 K and studied by time-resolved 2PPE at 30 K. Different annealing temperatures lead to a variety of structures that accompany crystallization of the initially amorphous clusters: porous clusters form upon D_2O absorption at 85 K (A), annealing to 120 K leads to compact amorphous clusters (a), successive annealing to 130 K, 145 K, and 149 K (b–d) result in ordered structures before desorption lowers the coverage significantly. Panel (C) depicts STM line scans of porous (dashed line) and compact (solid line) amorphous clusters. The porous clusters collapse upon annealing to 120 K as seen from the height reduction by 1 BL. The determination of real heights (given in BL) from apparent heights *h* requires a calibration of *h* because tunneling occurs through the water band gap. As detailed in ref. 16 this has been achieved by tunneling through the ice conduction band at 3.5 V. Panel (F) shows exemplary time-resolved 2PPE spectra for compact amorphous clusters. Likewise data have been taken for all reported structures. (Panels (A,C,F) reprinted from ref. 16 and (a-d) from ref. 31 with permission. Copyright 2007 by the American Physical Society.)

at this delay. However, as the electrons start at a higher energy in the case of porous clusters, their total energy gain within 300 fs is larger than in compact clusters.

The population decay of e_S is evaluated by integration of the 2PPE intensity at the energies of the solvated electron state for porous and compact amorphous cluster structures. The resulting population transients are displayed in the inset of Fig. 6 (top). Routinely, they are analyzed by a single exponential decay convolved with the temporal laser pulse profile (dashed curve). The resulting least square fits (solid lines) describe the experimental data well up to 150 fs. At larger time delays, the decay becomes non-exponential. This is a well-known result of the transient spatial constriction of the electron's wave function (*cf.* section 2), which leads to reduced transfer rates, which are reflected in the slowing down of the population decay. The exponential fits at early time delays ($t < 150$ fs), however, result in initial decay times of 36(5) fs and 50(5) fs for porous and compact amorphous clusters, respectively. This shows that the decay due to electron back transfer to the metal is, for porous clusters, 30% faster than for the compact ice. As introduced above, the transfer probability of solvated electrons is determined by a transient potential barrier at the interface. Having in mind that the porous clusters are higher than the compact ones (Fig. 5C) and considering that the electrons reside at the ice vacuum interface, a simple scaling of the potential barrier with the distance between electron and metal should lead to a faster electron back transfer for the *compact* ice clusters. Thus, the finding of a faster decay for *porous* clusters is counter-intuitive. The porous clusters have an average height of 4 BL, while compact clusters are 3 BL high as illustrated in Fig. 6 (bottom). As we observe a faster decay for porous ice, the qualitative difference in the potential barrier, rather than merely its width, needs to be considered. The faster decay for compact clusters asks for a less efficient screening by the porous cluster. As solvation and thus screening is driven by the water dipole, we attribute the faster decay in case of porous clusters to the lower dipole density resulting from the pores (Fig. 6, bottom).

Besides the population decay, the peak shift of the solvated electron feature e_S is also faster for the porous ice clusters compared to the compact ones as mentioned above. However, as will be shown in the next section, the explanation of this difference requires quantitative consideration of the electron transfer dynamics, as population decay and solvation are intimately linked by the transient evolution of the potential barrier at the ice–metal interface. We developed a model that simultaneously describes the peak shift and the population decay using energy-dependent transfer rates. It shows that the

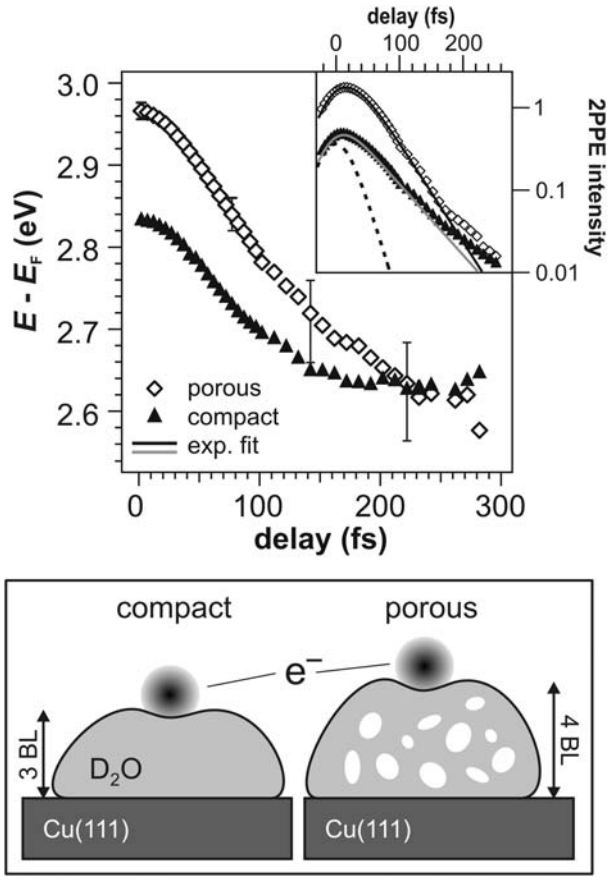

Fig. 6 Top: the main panel depicts the transient peak shift of the e_S feature for porous and compact amorphous ice clusters. The inset represents the transient population of e_S, which has been analyzed by integration of the 2PPE intensity within 2.58 and 3.17 eV. The dashed line marks the temporal profile of the laser pulse. Analysis of the electron transfer times within the first 150 fs results in a three times faster decay for porous clusters with a decay time of 36(5) fs compared to compact clusters which exhibit a decay time of 50(5) fs. Data have been taken at 30 K. (Reprinted from ref. 16 with permission. Copyright 2007 by the American Physical Society.) Bottom: a possible scenario explaining the observed differences in population decay for the two types of clusters. The excess electrons wave function and the D_2O clusters do not scale.

difference between the transient e_S peak shift for porous and amorphous clusters is explained by different electron transfer rates and not necessarily by different stabilization rates. However, the transient peak shift cannot be attributed to population decay only; both contributions have to be considered.

4. Competition of electron transfer and solvation

As shown in section 2, the electron dynamics at ice–metal interfaces occur *via* four fundamental steps; electron injection, localization, solvation, and simultaneous back transfer. These processes involve both a transient electron population of the excited state *and* a time-dependent change of the electron binding energy. In the previous sections, these dynamics have been analyzed and discussed separately. Yet, the concurrence of electron solvation and back transfer leads to a competition of these processes as (i) the transfer probability is reduced due to electron solvation resulting in wave function constriction of the excess electron and as (ii) electron solvation is impeded by a decreasing excited state population due to electron back transfer. In fact, this competition of solvation and transfer requires a combined analysis that takes into account time- *and* energy-dependent data. In the present section, the electron dynamics at two different ice–metal interfaces, D_2O/Cu(111) and D_2O/Ru(001), are compared so as to distinguish the substrate's influence from the ice impact on charge transfer and solvation. Compared to Cu(111), which exhibits a wide sp-band gap in the electronic band structure projected onto the surface plane that extends below the Fermi level of the metal, the Ru(001) band gap is three times narrower (as a function of parallel momentum) and the bottom of the gap lies more than 1 eV above the Fermi level. As will be shown further below, these differences in the electronic surface band structure affect the electron back transfer significantly. Also, the D_2O adsorption is different for the two respective metal surfaces: in contrast to Cu(111), where amorphous D_2O adsorbs in clusters for coverages below 2 BL and in layers for $\Theta > 2$ BL (*cf.* section 3), the first bilayer completely wets the Ru(001) surface.[32] By comparison of the electron dynamics at these two different ice–metal interfaces, the present section will demonstrate that electron transfer is characterized by energy-dependent charge transfer times $\tau(E)$, which results from a transient, interfacial potential barrier that changes upon electron solvation. The resulting increase in transfer times due to a reduced tunneling probability leads to an apparent energy shift of the peak maximum of the solvated electron distribution that adds to the peak shift, which originates from energetic stabilization due to the solvation process itself. As a result, a faster energy shift is observed, which depends on the electronic coupling to the metal substrate.

Before turning to the combined analysis of time- and energy-dependent data by the empirical model calculation, the peak shift and population decay for D_2O/Cu(111) and D_2O/Ru(001) is separately analyzed and discussed. Fig. 7 depicts the time-dependent peak shift of the solvated electron distribution (a) and its population decay (b) for D_2O multilayers (3–5 BL) on Cu(111) (diamonds) and Ru(001) (circles). Within the first few 100 fs, pronounced differences are encountered in peak shift and population decay. Thus, the substrate plays an important role in the ultrafast relaxation dynamics. However, the question is, whether the substrate impact is indirect (*i.e.* due to a structure modification of the adlayer) or direct (*i.e.* due to different electronic band structures influencing the electron transfer rates). Linear fits (dashed lines in Fig. 7a) to the time-dependent energy shift of the peak maximum of the solvated electron distribution[33] yield a three times faster peak shift of $\Sigma_S^{Ru} = -0.83$ eV ps^{-1} for D_2O/Ru(001) than for D_2O/Cu(111) ($\Sigma_S^{Cu} = -0.27$ eV ps^{-1}). The fit deviates from the data for $t > 300$ fs in the case of D_2O/Ru(001). Similarly, analysis of the population decay at early delays ($t < 300$ fs) using single exponential fits convolved with the laser pulses envelope (dotted curves) results in a more than four times faster initial transfer time $\tau_1^{Ru} = 34(5)$ fs for D_2O/Ru(001) than for D_2O/Cu(111) with $\tau_1^{Cu} = 140(5)$ fs. At larger delays ($t > 300$ fs), however, the charge transfer slows

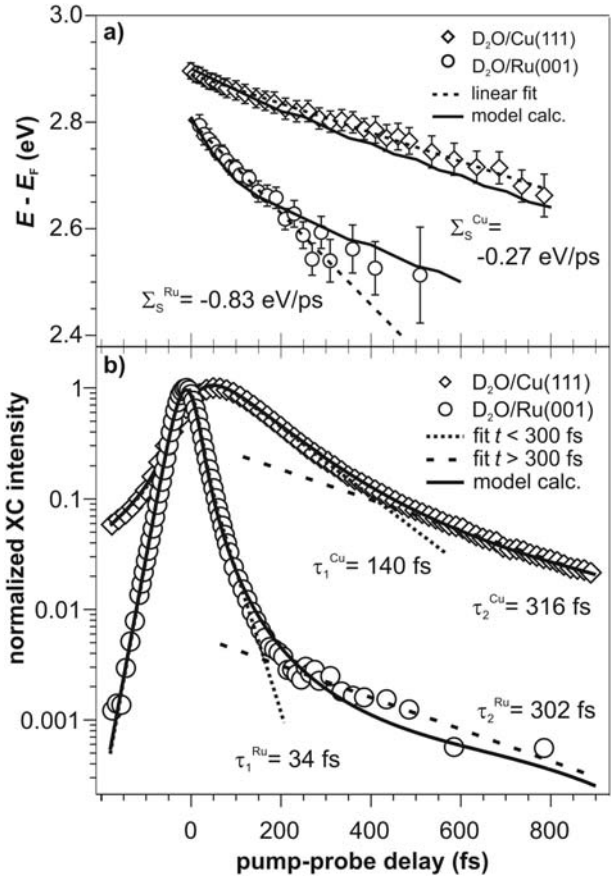

Fig. 7 Electron dynamics in amorphous D_2O layers on Cu(111) (diamonds) and Ru(001) (circles). Dashed and dotted curves are linear (top) or single exponential (bottom) least square fits to the data and solid lines result from the empirical model calculation. (a) Energy shift of the peak maximum of the solvated electron distribution. (b) Population decay of the solvated electron state (time dependence of the integrated e_S peak intensity). (Modified from ref. 36 with permission. Copyright 2006, the American Chemical Society.)

down and decay times become comparable: Single exponential fits (dashed lines) yield similar charge transfer times $\tau_2^{Ru} = 302(20)$ fs and $\tau_2^{Cu} = 316(20)$ fs for both substrates. Obviously, the electron transfer dynamics at the D_2O/Cu(111) and D_2O/Ru(001) interfaces can be separated into two different regimes: (a) at early delays ($t < 300$ fs), the electron transfer is significantly influenced by the substrate, resulting in different decay times τ_1^{Ru} and τ_1^{Cu}; (b) at larger delays ($t > 300$ fs) the substrate seems to play a minor role leading to similar charge transfer times $\tau_2^{Ru} \approx \tau_2^{Cu}$.

The upper panels of Fig. 8 illustrate these two regimes of charge transfer: For $t < 300$ fs (Fig. 8a) the excess electron still exhibits considerable wave function overlap with the metal substrate. Due to this wave function overlap the population decay is significantly influenced by the substrate's surface electronic band structure and density of states. As mentioned further above, the electronic properties of Cu(111) and Ru(001) differ significantly: the ruthenium crystal exhibits a higher density of states (DOS) up to $\sim$1.5 eV above the Fermi level resulting from its unoccupied d-bands. Furthermore, the Ru(001) substrate has, compared to Cu(111), a remarkably narrower sp-band gap in momentum space.[34,35] As discussed in detail in ref. 36, these differences in electronic properties of the substrates yield the explanation for the strongly varying transfer dynamics for $t < 300$ fs: the higher DOS of ruthenium favors electron population decay due to inelastic scattering; the narrower band gap of Ru(001) supports faster back transfer due to elastic scattering. Both attributes result in a faster electron population decay to the Ru(001) surface compared to the Cu(111) substrate as observed in the experiment. Thus, this charge transfer regime (a) will be referred to as *substrate-dominated*.

At larger delays ($t > 300$ fs), *i.e.* in the charge transfer regime (b), the electron dynamics are nearly identical for both substrates. As has been shown previously[15] and discussed in section 2, electron solvation leads besides the energetic stabilization to a wave function constriction that significantly reduces the wave function overlap of the excess charge with the metal substrate. This electron localization is due to the formation of a transient potential barrier at the interface (Fig. 8b) which results in a reduced decay probability of the electron population. Since this interfacial potential barrier increasingly screens the excess charge from the metal, the influence of the substrate's electronic properties is increasingly reduced as solvation proceeds. The rate-determining step for

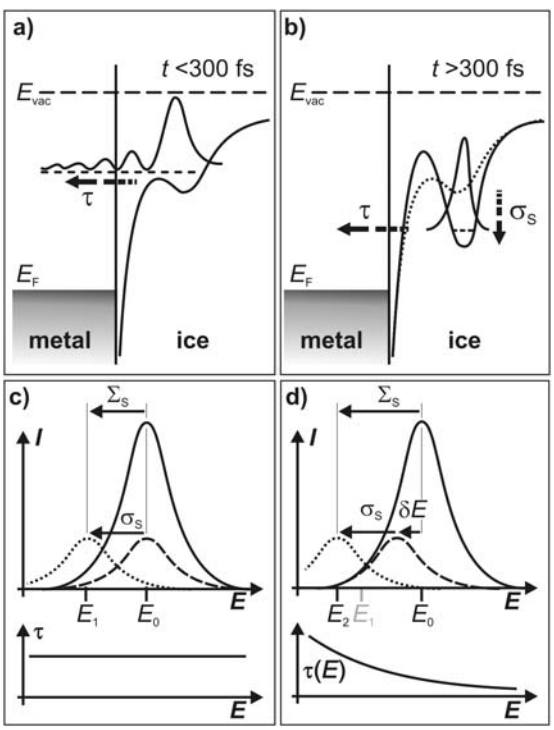

Fig. 8 (a) and (b): illustration of the substrate-dominated and barrier-determined transfer regimes, respectively. Electron solvation with the rate σ_S leads to the formation of an interfacial tunneling barrier that separates the electrons from the metal (Modified from ref. 36 with permission. Copyright 2006, the American Chemical Society.). (c) Constant transfer times τ do not change the peak position as a function of time. The observed peak shift Σ_S is similar to the energetic stabilization σ_S. (d) Energetically varying transfer times shift the peak maximum of the solvated electron distribution to lower energies (dashed curve). The observed peak shift Σ_S (dotted curve) is the sum of this peak shift δE and the stabilization σ_S.

electron transfer from the ice adlayer back to the respective substrate is no longer the metal band structure, but the tunneling probability through the potential barrier that has formed upon solvation. Based on our observation that charge transfer is substrate-dominated in the regime (a) and that the electron population decay slows down upon the transition to the regime (b) leading to similar ET rates for Cu(111) and Ru(001), we term the charge transfer regime at late delays ($t > 300$ fs) *barrier-determined*.

The observation of the transition between the substrate-dominated and the barrier-determined charge transfer regime is enabled by the simultaneity of electron transfer and solvation, as the latter leads to the formation of a transient potential barrier at the interface, which modifies the charge transfer rates. However, these varying transfer rates transiently reduce the electron population of e_S and thus influence the solvated electron distribution that undergoes further solvation. This competition of transfer and solvation is illustrated by the bottom panels of Fig. 8. First, we discuss the electron dynamics for the simple case of constant electron transfer times $\tau = const.$ (Fig. 8c) and then proceed to dynamically changing charge transfer times $\tau(E)$ (Fig. 8d). Given a distribution of solvated electrons around the energy E_0 (solid curve, Fig. 8c) and assuming a constant ET rate τ at all energies leads to a uniform (*i.e.* energy independent) population decay that results in an intensity decrease as illustrated by the dashed curve. In addition, electron solvation leads to a shift of the peak with the rate $\sigma_S < 0$ so that the solvated electron distribution is, at the time t, centered around the energy $E_1(t) = \sigma_S t + E_0$. Hence, in this scenario, the electron transfer would not influence the position of the peak maximum of the solvated electron distribution and an energy shift of the peak maximum would be observed with a rate $\Sigma_S = \sigma_S$.

However, as shown by the experiments above, the electron transfer rate changes with ongoing solvation due to the transient barrier, *i.e.* as a function energy E. The influence of these energy-dependent charge transfer times $\tau(E)$ is illustrated in Fig. 8d. The excess electrons at higher energies are less solvated, *i.e.* less screened from the substrate than the ones at lower energies. This results in decreasing lifetimes $\tau(E)$ with increasing energy (Fig. 8d, bottom). Compared to the initial solvated electron distribution (solid curve), the faster electron transfer at higher energies results in a redistribution of intensity in favor of low energies (dashed curve), *i.e.* in an additional energy shift δE that does not originate from the energetic stabilization due to solvation. In total, *i.e.* including the binding energy gain due to pure electron stabilization σ_S, the observed peak shift of solvated electron distribution occurs with a rate Σ_S and by the time t the peak maximum is centered at the energy $E_2(t) = \sigma_S t + E_0 - \delta E$ (dotted curve). In the line of these arguments, the significantly faster peak shift Σ_S^{Ru} observed for D_2O/Ru(001) compared to Σ_S^{Cu} (see Fig. 7a) cannot be necessarily attributed to a faster stabilization rate σ_S^{Ru} of the solvated electrons in D_2O/Ru(001), but originates from the differences in substrate electronic structure. The significantly different electron transfer dynamics for for Cu(111) and Ru(001) strongly suggest that differing $\tau^{Cu}(E)$ and $\tau^{Ru}(E)$ lead to the observed faster peak shift in the case of the Ru(001) substrate.

On the basis of the observations described above, we implemented a rate equation model for the electron transfer and solvation dynamics at ice–metal interfaces.[36] As a first approximation, a constant stabilization rate σ_S is assumed. In our model we introduce transfer times τ_0 that are (a) either energy-independent in the substrate-dominated regime (Fig. 8a) where only the electronic properties of the substrates influence the charge transfer rate or (b) exponentially rising as a function of binding energy of the solvated electrons in the barrier-determined regime (Fig. 8b). In the latter case the transfer rate is determined by the transient tunneling barrier (for further details on the model calculation see ref. 36). Using this approach we modeled the four data sets given in Fig. 7, *i.e.* peak shift and population decay for D_2O on both substrates: Cu(111) and Ru(001). The results of this empirical model calculation are given by the solid lines in Fig. 7a and b, respectively. Remarkably, our model reproduces all four datasets: the peak shift for D_2O/Cu(111) and the three times faster peak shift Σ_S^{Ru} is modeled including the slowing down after 300 fs. Also, the substrate-dominated decay for $t < 300$ fs, which differs for the two substrates, and the comparable, barrier-determined decay at late delays is reproduced for D_2O/Cu(111) and D_2O/Ru(001), respectively. The presented model calculations result in substrate-dominated transfer times $\tau_0^{Ru} = 20$ fs and $\tau_0^{Cu} = 67$ fs, which reflect the different electronic band structures of Ru(001) and Cu(111). In fact, the ratio $\tau_0^{Cu}/\tau_0^{Ru} = 3.3$ is comparable to the ratio of the band gap widths in momentum space $\Delta k^{Cu}/\Delta k^{Ru} = 3.2$ at energies of the solvated electron distribution. This agreement suggests that electron transfer is driven by elastic scattering, which requires a change of the parallel wavevektor Δk. In addition, the model yields comparable stabilization rates of $\sigma_S^{Ru} = -0.24$ eV ps^{-1} and $\sigma_S^{Cu} = -0.22$ eV ps^{-1} for both substrates, showing that the substrate itself hardly influences the pure solvation dynamics of the excess charge. In other words, the buildup of the solvation shell surrounding the excess electron is not modified by the metal substrate. As the stabilization rates σ_S^{Ru} and σ_S^{Cu} are comparable, the variation in the rates Σ_S of the observed peak shifts results, therefore, from the different energy-dependent transfer times $\tau(E)$ on the two substrates. This explains the differences of the additional peak shifts δE as illustrated by Fig. 8d.

The described model has also been applied to the electron dynamics in porous and compact amorphous ice clusters on Cu(111), which were introduced in section 3. There—similar to the comparison of D_2O/Cu(111) and D_2O/Ru(001) in the present section—the peak shifts differ for the two types of clusters (*cf.* Fig. 6). Applying the above described model to the time-dependent population decay and peak shift of porous and compact clusters shows that the differently energy-dependent transfer times $\tau(E)$ are again responsible for the variation of peak shifts, as will be shown in detail in a forthcoming publication.[29]

In summary, this section showed that the simultaneity of electron transfer and solvation gives rise to a competition of these two processes, as electron decay results in a reduced population that takes part in solvation, which—in turn—leads to enhanced screening for the excess charge from the metal and therefore to reduced decay rates. This competition can be

described by energy-dependent transfer times that ultimately lead to an additional contribution to time-dependent energy shifts of the solvated electron peak. With the aid of an empirical model calculation we could show that the three times faster peak shift in the case of D_2O/Cu(111) results mainly from such energy-dependence of the electron transfer rate and that the stabilization rate of electron solvation is actually comparable for both substrates, Cu(111) and Ru(001). We conclude that the competition of charge transfer and solvation is a substantial feature of electron dynamics at molecule–metal interfaces that should be considered in the discussion of peak shifts and population decay of interfacial electrons.

5. Conclusions

In this article we have presented a surface science approach to electron solvation dynamics at interfaces based on recent work on amorphous ice structures adsorbed on metal surfaces. This concept provides detailed insights into elementary processes and yields complementary information to related studies in the gas or liquid phase. In particular, the following advantages should be emphasized:

(i) the structure of the adsorbate layer can be controlled by different growth procedures using different substrates as a template. Thus well defined ice structures can be achieved, which can be characterized by various surface science techniques.[16] This allows to correlate the adsorbate structure with the corresponding electron dynamics;

(ii) the photoexcited excess electrons are injected from the metal substrate. The photohole is therefore completely screened by metal electrons and does not interact with the excess electron in the ice layer;

(iii) with the aid of femtosecond 2PPE spectroscopy the transient evolution of the electron binding energy and population can be probed directly in the time domain. Thereby the dynamics of all elementary processes can be studied, namely the charge injection across the interface, the subsequent electron localization in the ice and its energetic stabilization during solvation, as well as the dynamics of charge transfer back to the substrate;[14]

(iv) the localization of excess electrons is reflected by the corresponding changes of the dispersion along $k_{\parallel}$, which is accessible by angle-resolved 2PPE spectroscopy. Using time- and angle-resolved 2PPE the transient localization of the electron wave function can be monitored, which is driven by continuous reorientations of the surrounding polar water molecules;[36]

(v) the location of the solvation site in the interior or at the ice–vacuum interface can be determined by Xe overlayer experiments which probe the interaction between the Xe adatoms and the solvated electron wave function;

(vi) solvation and electron transfer processes are intimately connected, as the excited electron population continuously decays back to the metal substrate. Therefore, electron dynamics at polar adsorbate-metal interfaces may act as a model system to study interfacial charge transfer and the role of electronic coupling between localized charges and unoccupied states in a solid.

All issues mentioned above have been addressed in our studies on ultrafast electron transfer and solvation dynamics at amorphous ice–metal interfaces. Using LT-STM the various structural transformations of D_2O/Cu(111) from amorphous ice to crystalline ice have been characterized. For porous and amorphous ice clusters the solvated electrons are bound in surface sites at the ice–vacuum interface as demonstrated by Xe overlayer experiments. The substantially different initial electron transfer rates obtained for the two structures are attributed to different barrier heights, which depend on the efficiency of screening by the water dipoles. By changing the electronic structure of the underlying metal substrate (D_2O/Cu(111) and Ru(001), respectively) different regimes of electron transfer have been identified: in the initial regime of strong electronic coupling the transfer rate is dominated by the substrate electronic structure while at later times (with ongoing solvation) the buildup of the solvation shell determines the tunneling barrier and hence governs the transfer rate. This demonstrates the competition between two processes, namely electron solvation and localization in the adlayer on the one hand and charge transfer back to the metal substrate on the other hand. Both processes are essential for understanding the interfacial electron dynamics.

In summary, using a surface science approach to electron solvation we have obtained a comprehensive understanding of the elementary processes in the electron dynamics at amorphous ice–metal interfaces. Current new directions in this field include the trapping of excess electrons in crystalline ice structures at metal surfaces, where exceptional long lifetimes (up to minutes) are found and the dynamics of photoinjected electron spans over 17 orders of magnitude in time.[19] Electron solvation dynamics at adsorbate–metal interfaces directly address electron-induced nuclear reorientation processes which are at the heart of chemical reactions. The basic understanding of such electron–nuclear coupling and charge-transfer dynamics obtained here thus opens the perspective to achieve control over light-induced electronic and reactive processes at surfaces and electric currents in nanoscale electronic devices. Recent progress in this direction has been obtained for coherently controlled electric currents at metal surfaces,[37] spectroscopy of quasibound interface states at adsorbate–metal interfaces[38] as well as for adaptive spatial–temporal control of photoemission from nano-structured surfaces.[39]

Acknowledgements

This work was performed in collaboration with C. Gahl, D. O. Kusmierek, M. Mehlhorn, and K. Morgenstern. We would like to thank A. Nitzan, H. Petek, D. Truhlar and X-Y. Zhu for stimulating discussions. This work has been funded in part by the German-Israel-Foundation (GIF) and the Deutsche Forschungsgemeinschaft through SPP 1093 and Sfb 450.

References

1 A. Nitzan, *Chemical Dynamics in Condensed Phases*, Oxford University Press, Oxford, 2006.
2 T. R. J. Tuttle and S. Golden, *J. Phys. Chem.*, 1991, **95**, 5725.
3 A. L. Sobolewski and W. Domcke, *Phys. Chem. Chem. Phys.*, 2002, **4**, 4.

4 C. A. Kraus, *J. Am. Chem. Soc*., 1908, **30**, 1323.
5 E. J. Hart and J. W. Boag, *J. Am. Chem. Soc*., 1962, **84**, 4090.
6 F. H. Long, H. Lu and K. B. Eisenthal, *Phys. Rev. Lett*., 1990, **64**, 1469.
7 R. Laenen, T. Roth and A. Lauberau, *Phys. Rev. Lett*., 2000, **85**, 50.
8 J. V. Coe, G. H. Lee, J. G. Eaton, S. T. Arnold, H. W. Sarkas, K. H. Bowen, C. Ludewigt, H. Haberland and D. R. Worsnop, *J. Chem. Phys*., 1990, **92**, 3980–3982.
9 J. R. R. Verlet, A. E. Bragg, A. Kammrath, O. Cheshnovsky and D. M. Neumark, *Science*, 2005, **307**, 93.
10 L. Turi, W.-S. Sheu and P. J. Rossky, *Science*, 2005, **309**, 914.
11 N.-H. Ge, C. M. Wong and C. B. Harris, *Acc. Chem. Res*., 2000, **33**, 111.
12 U. Bovensiepen, *Prog. Surf. Sci*., 2005, **78**, 87.
13 J. Zhao, B. Li, K. Onda, M. Feng and H. Petek, *Chem. Rev*., 2006, **106**, 4402.
14 C. Gahl, U. Bovensiepen, C. Frischkorn and M. Wolf, *Phys. Rev. Lett*., 2002, **89**, 107402.
15 U. Bovensiepen, C. Gahl and M. Wolf, *J. Phys. Chem. B*, 2003, **107**, 8706.
16 J. Stähler, M. Mehlhorn, U. Bovensiepen, M. Meyer, D. O. Kusmierek, K. Morgenstern and M. Wolf, *Phys. Rev. Lett*., 2007, **98**, 206105.
17 B. Li, J. Zhao, K. Onda, K. D. Jordan, J. L. Yang and H. Petek, *Science*, 2006, **311**, 1436.
18 P. Szymanski, S. Garrett-Roe and C. B. Harris, *Prog. Surf. Sci*., 2005, **78**, 1.
19 J. Stähler, PhD thesis, Freie Universität Berlin, Germany, 2007, http://www.diss.fu-berlin.de/2007/479/.
20 J. Stähler, M. Meyer, D. O. Kusmierek, U. Bovensiepen and M. Wolf, *J. Am. Chem. Soc*., 2008, **130**, 8797.
21 *Nanoelectronics and Information Technology*, ed. R. Waser, Wiley-VCH, Weinheim, 2003.
22 B. O'Regan and M. Grätzel, *Nature*, 1991, **353**, 737.
23 A. Nitzan and M. A. Ratner, *Science*, 2003, **300**, 1384.
24 X.-Y. Zhu, *J. Phys. Chem. B*, 2004, **108**, 8778.
25 N. I. Hammer, J.-W. Shin, J. M. Haedrick, E. G. Dicken, J. R. Roscioli, G. H. Weddle and M. A. Johnson, *Science*, 2004, **306**, 675.
26 T. Shibaguchi, H. Onuki and R. Onaka, *J. Phys. Soc. Jpn*., 1977, **42**, 152, E_{gap} taken at a threshold of 50%.
27 D. Nordlund, H. Ogasawara, H. Bluhm, O. Takahashi, M. Odelius, M. Nagasono, L. G. M. Pettersson and A. Nilsson, *Phys. Rev. Lett*., 2007, **99**, 217406.
28 In fact, the competition of energy-dependent electron back transfer and electron solvation also contributes to the observed energy shift. This issue will be addressed in section 4.
29 M. Meyer, J. Stähler, D. O. Kusmierek, M. Wolf and U. Bovensiepen, *Phys. Chem. Chem. Phys*., 2008, **10**, 4932.
30 E. D. Sloan and C. A. Koh, *Clathrate Hydrates of Natural Gases*, Chemical Industries CRC Press, New York, 3rd edn, 2007.
31 M. Mehlhorn and K. Morgenstern, *Phys. Rev. Lett*., 2007, **99**, 246101.
32 G. Held and D. Menzel, *Surf. Sci*., 1994, **316**, 92.
33 The line shape of e_S has been attributed to an inhomogeneous distribution of solvation sites in the adlayer. See ref. 36.
34 A. P. Seitsonen, PhD thesis, Technical University Berlin, Germany, 2000, http://edocs.tu-berlin.de/diss/2000/seitsonen_ari.htm.
35 D. A. Papaconstantopoulos, *Handbook of the Band Structure of Elemental Solids*, Plenum Press, New York, 1986.
36 J. Stähler, C. Gahl, U. Bovensiepen and M. Wolf, *J. Phys. Chem. B*, 2006, **110**, 9637.
37 J. Güdde, M. Rohleder, T. Meier, S. W. Koch and U. Höfer, *Science*, 2007, **318**, 1287.
38 M. Rohleder, W. Berthold, J. Güdde and U. Höfer, *Phys. Rev. Lett*., 2005, **94**, 017401.
39 M. Aeschlimann, M. Bauer, D. Bayer, T. Brixner, F. J. García de Abajo, W. Pfeiffer, M. Rohmer, C. Spindler and F. Steeb, *Nature*, 2007, **446**, 301.

